Contents

C Exclusive and diffractive measurements

In this appendix, we are going to show the details of a few *Exclusive, Diffractive, and Tagging* processes during the Phase I EIC running, where some of these measurements are highlighted in the main text. Specifically, we assess the physics program of the Phase I EIC using state-of-the-art Monte Carlo generators, which are fully simulated through the ePIC detector. The goal is to provide a first quantitative estimate of the scientific impact achievable within the initial five years of operation. We discuss both the expected physics outcomes and what will remain out of reach during Phase I.

The section is structured as follows: section C.1 introduces the kinematics of Deep Inelastic Scattering (DIS) and defines all relevant variables, especially related to exclusive, diffractive, and tagging. As no experimental data are yet available, all physics studies are based on simulations with Monte Carlo generators, discussed in Section C.2. Section C.3 outlines the detailed running conditions of the first five years at the EIC. Backgrounds from both physics processes and machine effects are briefly addressed in Section C.4, followed by physics projections in Section C.5. Our conclusion is presented in Section C.7.

C.1 Kinematics

In the ePIC experiment at the EIC, event kinematics may be categorized in several ways: i) inclusive DIS variables, ii) tagging DIS variables, iii), diffractive variables, and iv) exclusive variables. For i), this has been covered from earlier sections. Below we show ii), iii), and iv).

C.1.1 Tagging variables

Generally, we study the spectator tagging process with proton or neutron detection in the final state from the nuclear breakup. For simplicity we write the following formulas for the case of proton detection; the formulas for neutron detection can be obtained by simple exchange $p \leftrightarrow n$. Note that the proton detections are mostly done by the B0 spectrometer and OMD, while neutrons are detected in the ZDC which has very different energy and momentum resolution.

For this paper, the tagging variables are mostly used in the case of deuteron spectator tagging. For details, see Ref. [66]. Specifically, there are two spectator kinematic variables for spectator proton (thus the subscript p): i) $p_{p\mathrm{T}}$ and ii) light-cone momentum fraction α_p.

- $p_{p\mathrm{T}}$ is the transverse momentum of the spectator in the lab frame.
- $\alpha_p = 1 + \frac{k^z}{E(\boldsymbol{k})}$, where $\mathbf{k}$ is the three-momentum of the spectator in the ion rest frame and $E(k)$ is the corresponding energy $\sqrt{|k|^2 + M_N^2}$. For deuteron, $0 < \alpha_p < 2$ where the longitudinal momentum of a spectator nucleon is bound by the total momentum of the deuteron.

Similar definitions can be derived for higher A nuclei. The case of neutron detection is described by the same formulas with $p \to n$.

C.1.2 Diffractive variables

In experimental terms, diffractive processes are identified by the presence of a rapidity gap — a region in the detector with no particle activity. These processes were extensively studied at HERA, where they were interpreted using the concept of *Pomeron exchange*. The Pomeron is modeled as a color-singlet object

composed of two gluons with zero spin, mediating the interaction between the virtual photon (emitted by the electron) and the hadron.

The key kinematic variables used to describe diffraction are:

- $x_P = \frac{x}{\beta}$: the fraction of the hadron's momentum carried by the Pomeron;
- $t = -(p' - p)^2$: the squared four-momentum transfer between the initial (p) and final (p') hadron states;
- $\beta = \frac{Q^2}{Q^2 + M_X^2 - t}$: where Q^2 is the virtuality of the photon and M_X^2 is the invariant mass squared of the diffractive hadronic system.

To analyze diffractive events, one needs the standard DIS kinematic variables (x and Q^2), along with measurements of the momentum transfer t and the properties of the final-state hadronic system. A crucial experimental signature is the presence of a rapidity gap and/or the direct detection of the scattered hadron. In cases where the diffractive final state M_X consists of a single particle or a well-defined state, the process is referred to as an *exclusive reaction*, reflecting the constrained and clean event topology.

C.1.3 Exclusive variables

Specifically, exclusive reactions refer to processes in which the entire final state of particles is detected, enabling precise reconstruction of the reaction dynamics. The "exclusivity" of such reactions imposes stringent requirements on detector acceptance. In these events, the scattered proton or nucleus typically loses only a small fraction of its momentum and often escapes undetected through the beam pipe. Ensuring exclusivity therefore relies on dedicated forward detection systems, including the far forward proton spectrometer, which consists of components such as the B0 detector, Roman pots, off-momentum detectors, and the zero-degree calorimeter (used for detecting neutral particles). Once exclusivity is established, it becomes essential to measure the relevant kinematic variables with high precision and broad acceptance. Of particular importance is the distribution of the momentum transfer t, which plays a key role in the imaging program.

There are several methods to reconstruct the momentum transfer variable t, each offering distinct advantages depending on the specific reaction under study. Broadly, these methods can be categorized into three types:

(i) *Hadron-only* method,

(ii) *Lepton + observable* method,

(iii) A *hybrid approach* that combines elements of both with imposed exclusivity.

For instance, in the case of deeply virtual Compton scattering (DVCS) on a proton, method (i) corresponds directly to Eq. 1. The reconstruction of p' can be based on B0 and/or the roman pots, where p is the nominal incoming proton beam momentum. Alternatively, t can be reconstructed using the four-momenta of the incoming electron, the scattered electron, and the produced real photon—this constitutes method (ii).

In practice, it is often beneficial to combine these approaches or use partial information from each to enhance the accuracy of t-reconstruction. This flexibility becomes especially important in regions of phase space where certain methods are limited or inapplicable—for example, when the outgoing heavy nucleus is not detectable.

Beyond the three primary reconstruction methods, further improvements can be made by exploiting the differences among them to suppress events with poor resolution —though this comes at the cost of reduced statistics. Another recent proposal suggests reconstructing the momentum transfer t along a specific projected direction to mitigate the impact of detector smearing [67]. This approach can be used in conjunction with, and as an enhancement to, the traditional methods outlined above. Such developments are particularly crucial for the imaging program of heavy nuclei at the highest collision energies at the EIC.

C.2 Monte Carlo Generators

- **PYTHIA 8** PYTHIA simulates high-energy particle collisions based on the framework of Quantum Chromodynamics (QCD) and electroweak theory, capturing both perturbative and non-perturbative aspects of the interactions. The simulation begins with a hard scattering process between partons (quarks or gluons), calculated using perturbative QCD matrix elements. This is followed by parton showers, where initial- and final-state radiation accounts for the emission of additional gluons and quarks due to QCD bremsstrahlung, approximated using DGLAP evolution equations. As the partons evolve and separate, hadronization occurs via the Lund string model, where color field lines between partons stretch into strings that eventually break into color-neutral hadrons. PYTHIA also includes models for multiparton interactions (MPI) and beam remnants, which are especially important at high energies. The result is a full event record of particles that reflect both the quantum field theoretical dynamics and the complex structure of the colliding hadrons.

- **Sartre** A Monte Carlo model for gluon saturation physics via exclusive VM photo- and electroproduction in photon-nucleus collisions. The model applies nonlinear gluon evolution to calculate the scattering amplitude of a color-dipole, provided by the photon, and a target at a given impact parameter. Based on the Good-Walker paradigm, the model can predict both coherent and incoherent VM production, where the coherent process probes the average gluon density and the incoherent process is sensitive to the density fluctuation. Also known as the hot-spot model, the mechanism in incoherent VM production implements fluctuations of the parton and nucleon positions inside of a nucleon and a nucleus, respectively, their gluon densities, and their associated saturation scale Q_s. For this analysis, the comparisons to the measured data are based on Refs. [68, 69]. This model is only valid for parton momentum fraction $x_{\text{parton}} < 0.01$, while it is compared with the STAR data at $x_{\text{parton}} \approx 0.03$. The small mismatch to the data's kinematics needs to be taken into account when interpreting the data.

- **BeAGLE** A general-purpose electron-nucleus (e+A) model, BeAGLE [70] is used for the description of incoherent photoproduction only. Details of this model are given in Refs. [66, 70–73]. The comparison to heavy-ion (A+A) UPC cross sections is done by correcting the photon flux from e+A to A+A, where the e+A photon flux is based on PYTHIA 6 [74] and the A+A UPC photon flux is provided by the STARlight generator. BeAGLE uses the FLUKA program [75, 76] to describe neutron emission from nuclei. For this analysis, the comparisons to the measured data are based on Ref. [70].

- **DEMPgen** DEMPgen is a modular event generator for **D**eep **E**xclusive **M**eson **P**roduction reactions [77]. DEMPgen utilizes parameterizations of theoretical model to produce absolutely-normalized event samples. This enables a quick and direct projection of event rates. DEMPgen is capable of producing events in both fixed target and colliding beam kinematics. In collider kinematics, events for the DEMP reaction $p(e, e'\pi^+ n)$, of interest for pion form factor studies, up to a Q^2 of 35 GeV^2. This kinematic range is limited by the current parametrization of Regge-based models utilized in the event generator. Upgrades to DEMPgen, including the expansion of this Q^2 range, are ongoing.

Year	Species	Energy (GeV)	Lumi./year (fbˆ-1)	e- pol.	p/A pol.	Selected processes in this work
1	eRu/Ag	10x115	0.9	No (commissioning)	N/A	Diffractive DIS
2	eD	10x130	11.4	LONG	NO	Tagged DIS with spectator tagging
	ep		4.95-5.33		TRANS	DVCS, DVMP, DEMP
3	ep	10x130	4.95-5.33	LONG	TRANS and/or LONG	DVCS, DVMP, DEMP
4	eAu	10x100	0.84	LONG	N/A	Diffractive Vector-Meson
	ep	10x250	6.19-9.18		TRANS and/or LONG	DVCS, DVMP, DEMP
5	eAu	10x100	0.84	LONG	N/A	Diffractive Vector-Meson
	eHe3	10x166	8.65		TRANS and/or LONG	Tagged DIS with spectator tagging

Table C.1: Phase-I ePIC running plan with beam species, energies, luminosities, polarizations, and selected processes.

- **lAger** known as Argonne Generic l/A Event Generator is a highly adaptable and modular Monte Carlo simulation framework developed to model a broad range of lepton- and photon-induced reactions on both nucleons and complex nuclei [78]. Designed with versatility in mind, lAger supports simulations across a wide kinematic regime, encompassing both fixed-target configurations, typical of experiments at facilities such as Jefferson Lab, and collider geometries, such as those envisioned for the upcoming EIC. Significant recent development has focused on enhancing the capabilities of lAger to support Deeply Virtual Meson Production (DVMP) processes, which are of central importance in probing the partonic structure of hadrons and nuclei via GPDs. The generator has been adapted to incorporate models for exclusive vector meson production, with specific attention given to the production of heavy quarkonia such as the J/ψ. Studies of J/ψ production have primarily focused on the kinematic regime defined $1 < Q^2 < 10$ GeV^2, which is particularly relevant for probing the transition between non-perturbative and perturbative QCD dynamics.

- **EpIC** EpIC [79, 80] is a state-of-the-art Monte Carlo event generator developed for the study of exclusive processes. It is built on the PARTONS platform [81, 82], which provides a modular and extensible software architecture, allowing for the integration of a wide range of theoretical models describing the partonic structure of the nucleon. EpIC currently supports a range of exclusive reactions, including Deeply Virtual Compton Scattering (DVCS), Time-like Compton Scattering (TCS), Deeply Virtual Meson Production (DVMP) with π^0, and Double Deeply Virtual Compton Scattering (DDVCS). It also features the implementation of radiative corrections. EpIC is well-suited for both the analysis of existing experimental data and for impact studies, particularly in the context of future experiments at EIC [83].

C.3 Phase I EIC running schemes

The initial planning of the Phase I EIC is summarized in Table. C.1. The setup is based on both the physics impact and the early commissioning of the newly built accelerator machine. That said, the plan may be subject to change depending on the development of the project as well as the interest from the ePIC collaboration. For now, we make physics projection studies based on this table only.

The initial year focuses on commissioning the detector and accelerator systems, using electron-ion collisions involving Ruthenium or Silver nuclei at 10x115 GeV. While no electron polarization is available in this first year, the delivered integrated luminosity is expected to be approximately 0.9 fb^{-1}. The primary physics focus during this period is on (diffractive) DIS on nuclei, which marks the first eA collisions at a high-energy collider. This will lay the groundwork for future precision studies on the gluon saturation phenomenon - which was also one of the "*Day 1*" measurements from the EIC White Paper.

In the second year, the EIC will begin its core physics program with collisions involving deuterons and

protons at a beam energy of 10x130 GeV. Electron polarization will be longitudinal, while the deuteron beam will be unpolarized and the proton beam transversely polarized. The expected annual luminosities are 11.4 fb^{-1} for eD and 4.95 – 5.33 fb^{-1} for ep. This year's program includes spectator-tagged DIS, which is crucial for measuring the free neutron structure, along with deeply virtual Compton scattering (DVCS), deeply virtual meson production (DVMP), and deeply exclusive meson production (DEMP) on protons. These processes are instrumental for probing the nucleon and meson structure in terms of GPDs.

The third year continues with electron-proton collisions at the same energy configuration of 10×130 GeV. Both beams will now be polarized – electrons longitudinally, and protons transversely and/or longitudinally. The integrated luminosity is expected to remain in the 4.95 – 5.33 fb^{-1} range. This run will focus on high-precision studies of DVCS, DVMP, and DEMP, leveraging both beam polarizations to perform spin-dependent measurements, which will further study the proton spin decomposition, especially the quark and gluon Orbital Angular Momentum.

In the fourth year, the collider will diversify its physics reach by incorporating gold nuclei alongside protons. Gold beams will be collided with electrons at 10×100 GeV, while the ep configuration will reach up to 10×250 GeV. The annual luminosities are projected to be 0.84 fb^{-1} for eAu and 6.19 – 9.18 fb^{-1} for ep. Electron beams remain longitudinally polarized, while the protons will be polarized either transversely or longitudinally. This year's program will enable studies of nuclear effects in exclusive processes such as diffractive vector meson production for the gluon spatial distribution in heavy nuclei, as well as continued exploration of DVCS, DVMP, and DEMP in both ep and eA collisions.

Finally, the fifth year will extend the program to additional nuclear targets, including helium-3 and gold, at 10×166 GeV and 10×100 GeV, respectively. Luminosities of 8.65 fb^{-1} for eHe3 and 0.84 fb^{-1} for eAu are expected. Electron beams remain longitudinally polarized, and the He3 beams will again use transverse and/or longitudinal polarization where applicable. The focus this year includes precision diffractive vector meson production in heavy nuclei and DIS with spectator tagging to measure the spin-dependent structure function of the neutron, which are essential for studying the partonic structure of nuclei and nucleons. These measurements will provide valuable insight into both nucleonic and nuclear structure and mark the culmination of a diverse and impactful initial running phase of the EIC.

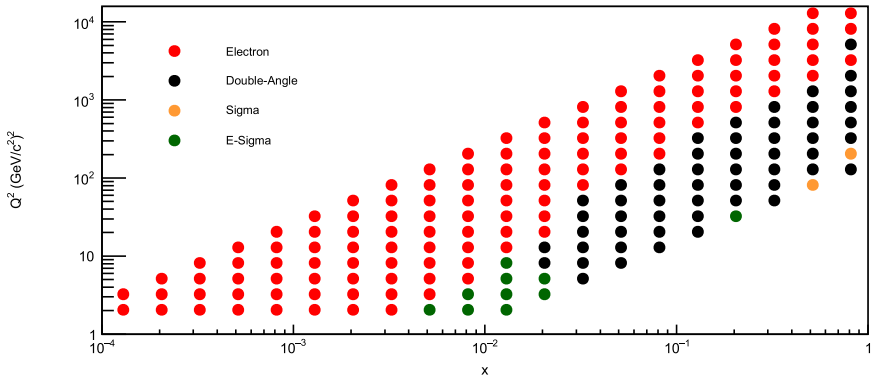

Figure C.1: Highest efficiency algorithm for each kinematic bin. Efficiency is determined by the number of events reconstructed in the correct bin using each reconstruction algorithm over the true number of events in the bin calculated using MC information.

C.4 Analysis techniques, Backgrounds, and Uncertainty

For most of the ePIC physics analyses, scattered electron is reconstructed not only for the DIS kinematic variables, but also physics variables. The exception may be the photoproduction process, which we do not discuss in this paper. Specifically for the exclusive physics program, the event activities/occupancies in the main ePIC detector are very low, mostly 1-2 particles. The general event selection will be as follows:

- Good scattered electron candidates that satisfy i) $0.9 < E/p < 1.2$ and ii) $18 < E - P_z < 22$ GeV or similar. Depending on analyses, the scattered electron can be reconstructed via a combination of EEMC cluster for energy measurement and tracking for the momentum measurement. Particle Identification (PID) detectors are not used in this study, which is expected to further improve the electron purity.
- Phase space selection on x, y, W, and/or Q^2.
- Event activity or multiplicity is limited to only the exclusive final-state, e.g., $N_{track} < 3$ for exclusive ϕ meson production. In addition, for proton beams, missing mass cut is also placed to further improve the exclusive event purity and resolutions.
- For protons and light ion beams, far-forward detectors will reconstruct the scattered protons and nucleons from nuclear breakup, respectively. We require a B0, RP, or OMD track by ensuring at least one hit per layer in their respective subsystem.
- For heavy nuclei, event rejection by veto activities in the FF system is used. We reverse the selection criteria for each subsystem in the FF above, and we require none of them has a signal track in order to veto this event.

In the current study, we estimate the impact from residue inclusive DIS events that survive our exclusive event selections. It is found that the exclusivity selection has an efficiency of more than 99% ,depending on the final-state. For example, for DVCS, the physics background can come from π^0 production with two photons merged into one, which is estimated to be around 1% at the lowest energy 5x41 GeV. For early science energies, this is much less than 1%.

Furthermore, Events with resonances in the final state, e.g., vector-meson, generally has even higher exclusive event efficiency due to the selection on the mass. For instance, the DVMP with J/ψ can have a residue DIS background where low multiplicity events that proton can be excited and become neutron However, the exception is the eAu diffractive ϕ production where the dominate background comes from incoherent ϕ production. The remaining background events is on the order of 1% but its highly t dependent. See results later in Section C.5. Other non-physics backgrounds, e.g., from the machine, were not considered for most analysis except for DVCS and π^0.

At the current stage, since no ePIC detector system is built, estimating systematic uncertainties based on the instrumentation can be difficult and unrealistic. Therefore, our approach is to evaluate systematic uncertainty in a limited fashion, with either projected performance of a detector or uncertainties related to the analysis from previous experiences, e.g., HERA. Below are a few major uncertainty sources that are currently under consideration:

- Integrated luminosity - 1%
- Event and track selections
- Selection on signal extraction

DIS & physics (Q^2 >1 GeV^2)	Machine	
DVCS	3% for DIS and < 1% from π^0	
DVπ^0P	0% low t and 60-100% for high t	
DEMP	0.012% for DIS	
DVMP	<40% but can be removed by mass fits	
eAu ϕ	~1% incoherent	
eHe3	Photoproduction (not studied here)	

Table C.2: Current estimates of contamination from DIS event and machine (all sources - beam gas, synchrotron etc) backgrounds for all of the exclusive, diffractive and tagging analyses described in this section.

- Incoherent diffractive contamination

Table. C.2 summarizes the potential contamination from DIS and machine backgrounds for each analysis based upon the current simulations. In Table. C.3, the dominant systematic uncertainty sources are listed for each analysis based on past experiences. This is by no means a rigorous method to evaluate systematic uncertainty, which will be only possible after the detector is built, but it is a way to anticipate potential uncertainty that could arise in the analysis level. Follow-up pseudo-analysis will be performed accordingly to quantify the systematic uncertainty based on detector and physics simulations.

	Dominant systematics source	Estimates
DVCS	BH interference?	
DVπ^0P	cluster merging	
DEMP	Scale uncertainty	12%
DVMP	Background estimation and efficiency	
eAu ϕ	Incoherent background and unfolding	
eHe3	Far-forward mistagging rate?	

Table C.3: Dominant sources of systematic errors on the exclusive, diffractive and tagging measurements described in this section. These estimates are based upon past experience from the closest comprable existing measurements.

C.5 Results

All results are reported in terms of phase I EIC luminosity; if possible, we can report the ultimate energy with higher luminosity.

C.5.1 Imaging program of protons

A central objective of the EIC physics program is to explore the three-dimensional structure of nucleons and nuclei. This structure can be accessed through Generalized Parton Distributions (GPDs), which are experimentally probed via exclusive processes such as Deeply Virtual Compton Scattering (DVCS) and Deeply Virtual Meson Production (DVMP). Among these, DVCS provides the cleanest access to GPDs

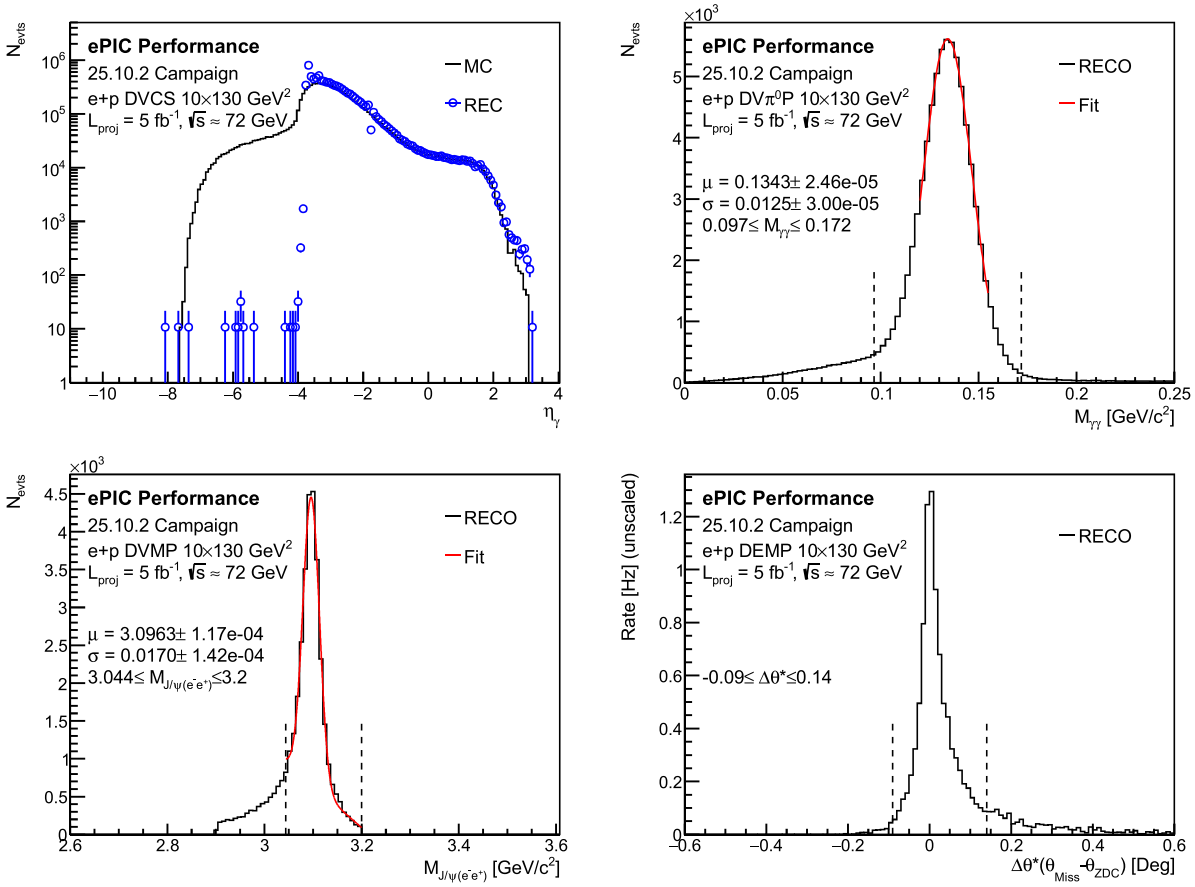

Figure C.2: Reconstructed distributions of key observables for each deep exclusive process: (top left) Pseudo-rapidity distribution of the DVCS photon. (top right) Reconstructed π^0 invariant mass distribution for exclusive π^0 production. (bottom left) Reconstructed J/ψ invariant mass distribution for DVMP. (bottom right) Angular difference between the reconstructed neutron and the missing momentum calculated from the combined scattered electron and pion.

and is particularly sensitive to chiral-even GPDs through its cross section, allowing for a detailed spatial imaging of quark distributions within the nucleon. In contrast, DVMP involving J/ψ mesons serves as a powerful probe of the gluon spatial distribution. Complementary information is provided by hard exclusive π^0 production (DVπ^0P), which is sensitive to chiral-odd GPDs related to quark transversity distributions. Furthermore, measurements of meson form factors through Deep Exclusive Meson Production (DEMP) offer insights into the internal structure of pions and their role as Goldstone bosons, which is particularly relevant for understanding the mechanism of mass generation in QCD. In this section, we examine four selected physics channels to illustrate the scientific potential of the EIC ePIC detector during its first five years of operation.

To demonstrate the detector's ability to realize this physics program, detailed simulations were performed for representative exclusive processes. To evaluate the detector acceptance, performance, and efficiency for each physics channel, reconstructed distributions of key observables for the deep exclusive processes are shown in Fig. C.2. The top-left panel presents the pseudo-rapidity distribution of the DVCS photon, where the reconstructed variable are compared with the Monte Carlo truth. The sharp drop below $\eta \sim -3.5$ corresponds to the limited acceptance of the central detector, while good agreement is observed within the central detector coverage. The top-right panel shows the reconstructed invariant mass distribution of

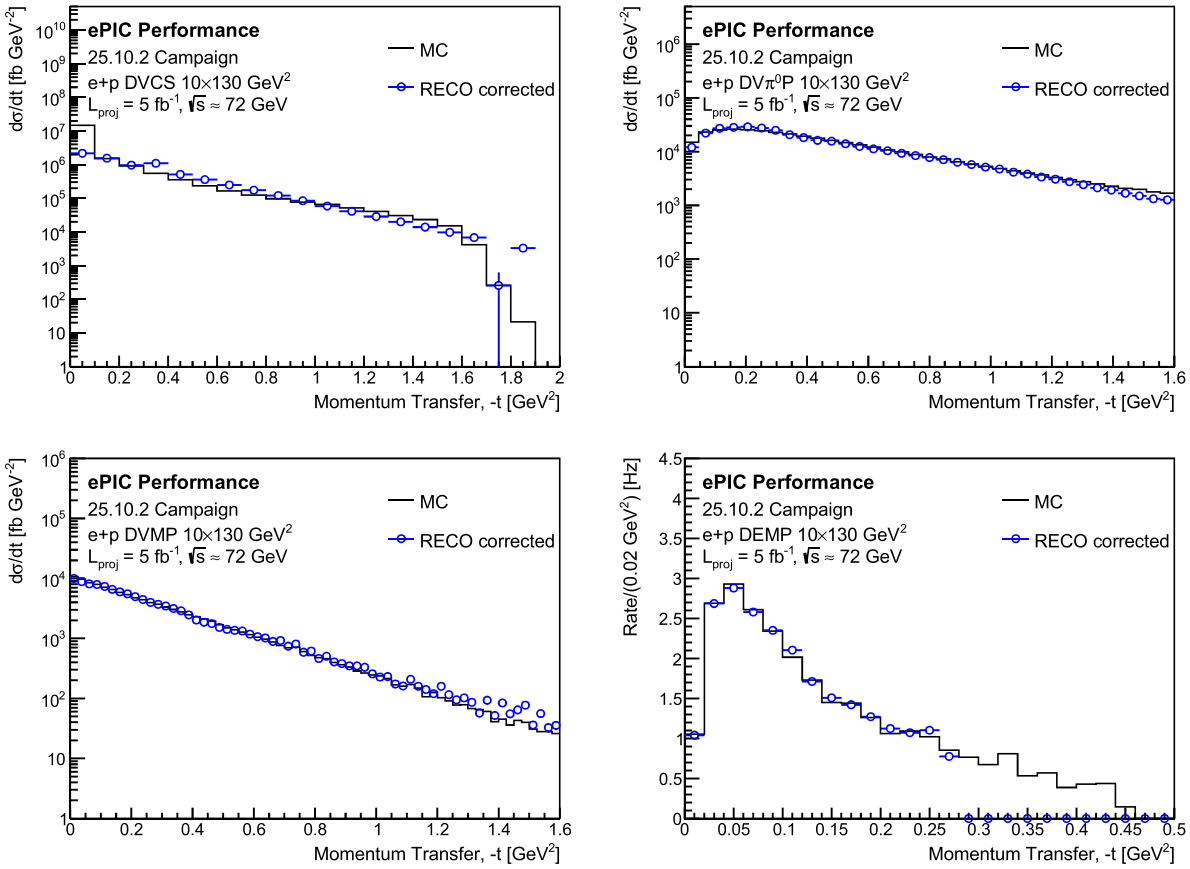

Figure C.3: Corrected t-distributions for each deep exclusive process, accounting for acceptance and efficiency effects: (top left) DVCS. (top right) Exclusive π^0 production. (bottom left) DVMP J/ψ production. (bottom right) DEMP.

the π^0in exclusive π^0 production, which includes the effects of calorimeter resolution. The distribution peaks at the nominal π^0 mass and exhibits a long tail toward lower masses due to energy smearing. The bottom-left panel displays the reconstructed J/ψ invariant mass distribution for DVMP events. Similarly, the distribution peaks at the nominal J/ψ mass with a relatively narrow width, indicating good mass resolution. The bottom-right panel shows the angular difference between the reconstructed neutron in the ZDC and the missing momentum calculated from the combined scattered electron and pion. In other words, it compares the reconstructed neutron impact position with the expected one for a true DEMP event. The distribution being close to zero and narrow demonstrates that neutron reconstruction is highly effective. Overall, the key observables for each deep exclusive process are well reconstructed, indicating reliable detector performance within the expected acceptance regions.

Following the validation of reconstruction performance, exclusivity requirements are imposed to select pure samples of exclusive events for cross-section determination. Each physics channel satisfies the requirements to be identified as an exclusive process for cross-section evaluation. The exclusivity criteria are as follows: (1) a well-identified scattered electron; (2) a well-reconstructed key observable — a photon for DVCS, a π^0 for DVπ^0P, J/ψ for DVMP, and a neutron for DEMP; (3) a well-identified scattered proton; and (4) complete reconstruction of all final-state particles. Once these requirements are met, the distribution of the squared momentum transfer, t, can be calculated, as shown in Fig. C.3, and compared with the Monte Carlo truth. The results have been corrected for detector acceptance and efficiency, and normalized by

the integrated luminosity. The current version of the figure uses only the scattered proton information to compute $t_{\mathrm{BABE}} = (p - p')^2$. The reconstructed t-distribution exhibits a dip corresponding to the limited acceptance of the far-forward detectors; however, this gap can be mitigated by incorporating the reconstructed key observable to calculate $t_{\mathrm{eXBE}} = (p - p'_{\mathrm{corr}})^2$. In the case of DEMP, the t_{eXBABE} method is used to calculate t as this provides the most accurate results for this channel. The resulting t-distributions provide the foundation for spatial imaging of quark and gluon distributions within the nucleon through Fourier transformation and the extraction of pion form factors, F_π as seen in Fig. C.4. Further details on the $DV\pi^0P$ and DEMP measurements, including the process of extracting F_π can be found in the ePIC analysis notes for these channels [84, 85].

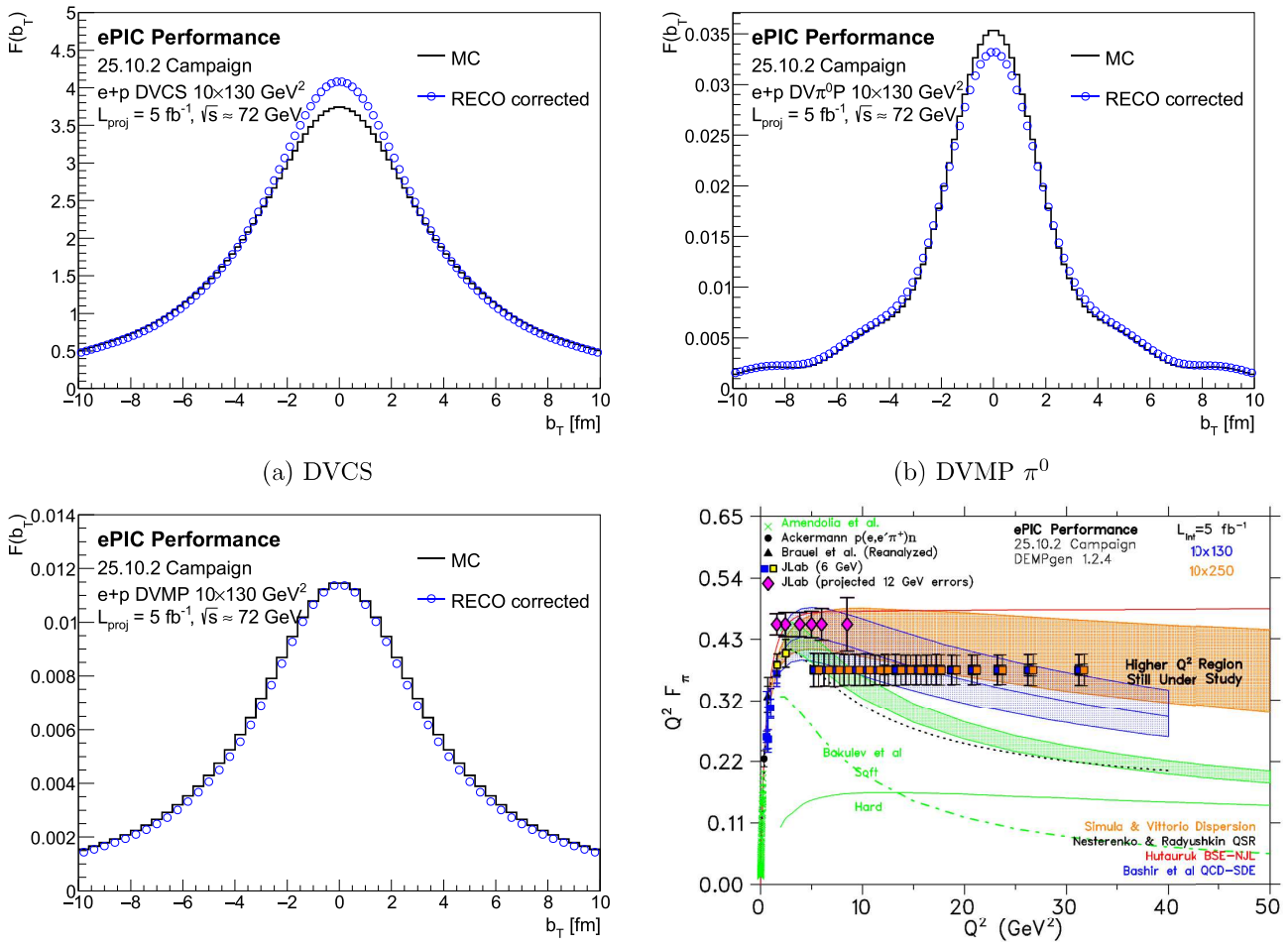

(a) DVCS

(b) DVMP π^0

(c) DVMP J/ψ

(d) DEMP

Figure C.4: Fourier Transforms of the t distributions seen in Fig C.3 for DVCS (top left), exclusive π^0 production (top right) and DVMP J/ψ production (bottom left). Projected uncertainties for F_π extraction from DEMP measurements are also shown (bottom right). Note that for DEMP, the y-positioning of projected points is arbitrary but the error bars represent the projected errors for these points.

C.5.2 Tagged DIS on deuteron

Proton structure functions are routinely measured in inclusive deep-inelastic scattering. However, structure functions measured on a neutron target can provide additional insight related to quark-flavor sep-

aration and enable further study into the onset of nuclear modifications to structure functions in light nuclei. Accessing neutron structure functions is experimentally challenging due to a lack of pure neutron beams/targets. A successful approach has been implemented in fixed-target experiments using spectator-tagged deep-inelastic scattering on a deuterium target, where the proton spectator is used to determine the relative momentum between the nucleons to identify a configuration where the nucleons are quasi-free [86–89]. However, the fixed-target kinematics make it difficult to achieve $p_{T,spectator} \lesssim 70$ MeV/c. In the collider kinematic environment at the EIC access to a kinematic region where $p_{T,spectator} \sim 0$ MeV/c enables application of pole extrapolation methods with smaller uncertainties to extract free neutron structure functions from the lightly bound deuteron by exploiting the behavior of the deuteron wave function near its pole [66, 90–92]. Additionally, neutron-tagged events can be used to extract free proton structure which can then be compared to measurements in electron + proton collisions with the same kinematics at the EIC, allowing for control over systematics associated with the pole extrapolation method itself.

In ePIC, simulations are performed using BeAGLE electron + deuteron DIS events passed through the full ePIC detector simulation and reconstruction framework. In the tagged-proton case, protons are reconstructed using the off-momentum detectors, while the tagged-neutron events are reconstructed using the zero-degree calorimeter.

The first step in this analysis is extraction of the tagged-deuteron cross section:

$$\begin{aligned} \mathrm{d}\sigma = \mathrm{Flux}(x, Q^2)\mathrm{d}x\mathrm{d}Q^2\frac{\mathrm{d}\phi_{e'}}{2\pi} \\ \times\sigma_{\mathrm{red},d}(x, Q^2, \alpha_p, p_{pT}, \phi_p)\mathrm{d}\Gamma_p, \end{aligned} \tag{12}$$

where $\mathrm{Flux}(x, Q^2)$ is the photon flux defined as:

$$\mathrm{Flux}(x, Q^2) \equiv \frac{2\pi\alpha_{em}^2 y^2}{Q^4(1-\epsilon)x}. \tag{13}$$

Here, α_{em} is the fine structure constant and ϵ is the virtual photon polarization parameter:

$$1 - \epsilon = \frac{y^2}{1 + (1-y)^2} + \mathcal{O}\left(\frac{x^2 m_N^2}{Q^2}\right). \tag{14}$$

The last term in Eq. (12) is the invariant phase space element $\mathrm{d}\Gamma_p$ which can be written as:

$$\mathrm{d}\Gamma_p = [2(2\pi)^3]^{-1}\frac{\mathrm{d}\alpha_p}{\alpha_p}\frac{\mathrm{d}p_T}{2}\phi_\mathrm{p}. \tag{15}$$

Figure C.5 shows the tagged-deuteron cross section for a single (x, Q^2, α_p) bin for tagged protons (top) and tagged neutrons (bottom).

Once this distribution is obtained, the inverse of the deuteron pole factor ($S_d(p_{pT}, \alpha_p)[\mathrm{pole}]$) is applied to remove the pole and acquire the tagged-*nucleon* cross-section ($\sigma_{red,n}$) which can then be used to perform the pole extrapolation and can be written as:

$$\sigma_{red,n} = \frac{\bar{\sigma}_{\mathrm{red},d}(x, Q^2)}{[2(2\pi)^3]S_d(p_{pT}, \alpha_p)[\mathrm{pole}]}, \tag{16}$$

where the deuteron pole factor is:

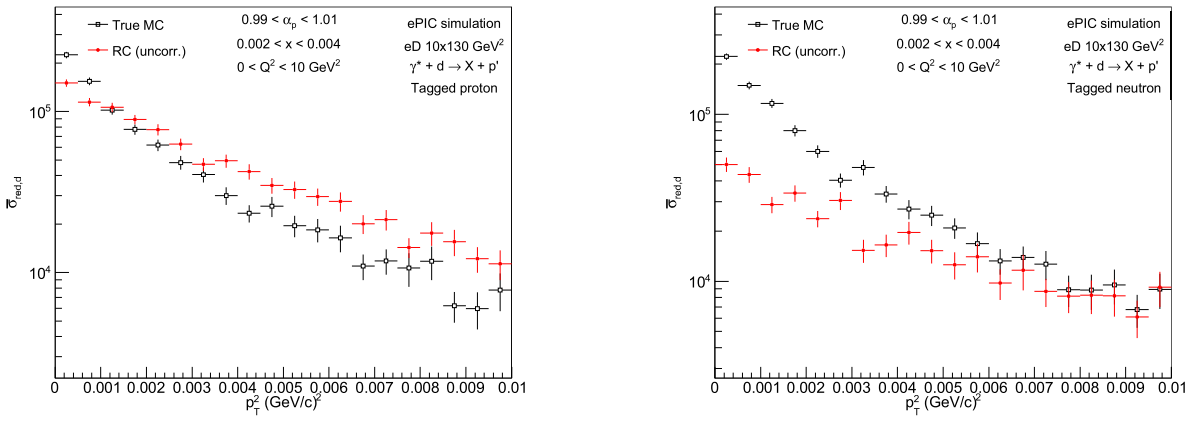

Figure C.5: Tagged-deuteron reduced cross-section from events with a tagged spectator proton (top) and neutron (bottom).

$$S_d(p_{pT}, \alpha_p)[\text{pole}] = \frac{R}{\left(p_{pT}^2 + a_T^2\right)^2}, \tag{17}$$

$$a_T^2 = m_N^2 - \alpha_p(2-\alpha_p)\frac{M_d^2}{4}, \tag{18}$$

$$R = \alpha_p^2 m_N \Gamma^2 (2-\alpha_p). \tag{19}$$

All factors in Eq. (12)-(19) can be calculated from kinematics of the scattered electron and the spectator nucleon, except for the residue of the nucleon pole factor of the nonrelativistic deuteron wave function Γ which has to be calculated from theory, or obtained from an experiment. The value used in this study is $\Gamma = 0.007885$ GeV. All Eq. (12)-(19) and the value of Γ are taken from Ref. [66]. Examples of the nucleon cross sections, in the same (x, Q^2, α_p) bin as Fig. C.5, are shown in Fig. C.6.

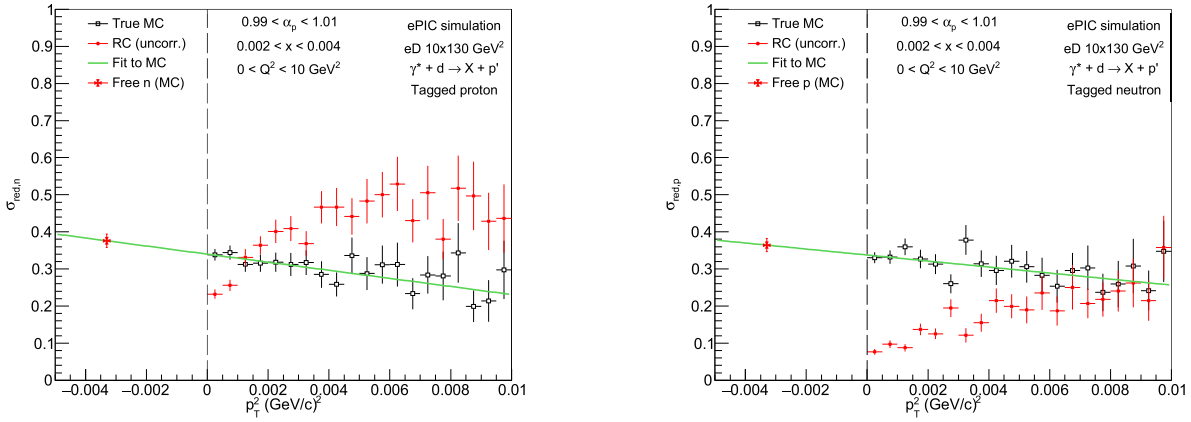

Figure C.6: Spectator proton (top) and neutron (bottom) cross-section after removal of pole from deuteron reduced cross-section. This distribution is then fit with a straight line to perform the pole extrapolation to find the on-shell point where the nucleon is unbound.

A linear fit is performed and the fit is evaluated at the location of pole where $p_{T,spect}^2 \to -a_T^2$. This

extrapolated value is the reduced cross-section on the quasi-free active nucleon (tagged proton means extraction of the *neutron* reduced cross-section). The full set of these reduced cross-section values in bins of (x, Q^2) and for $\alpha_p \sim 1.0$ are shown in Fig. C.7.

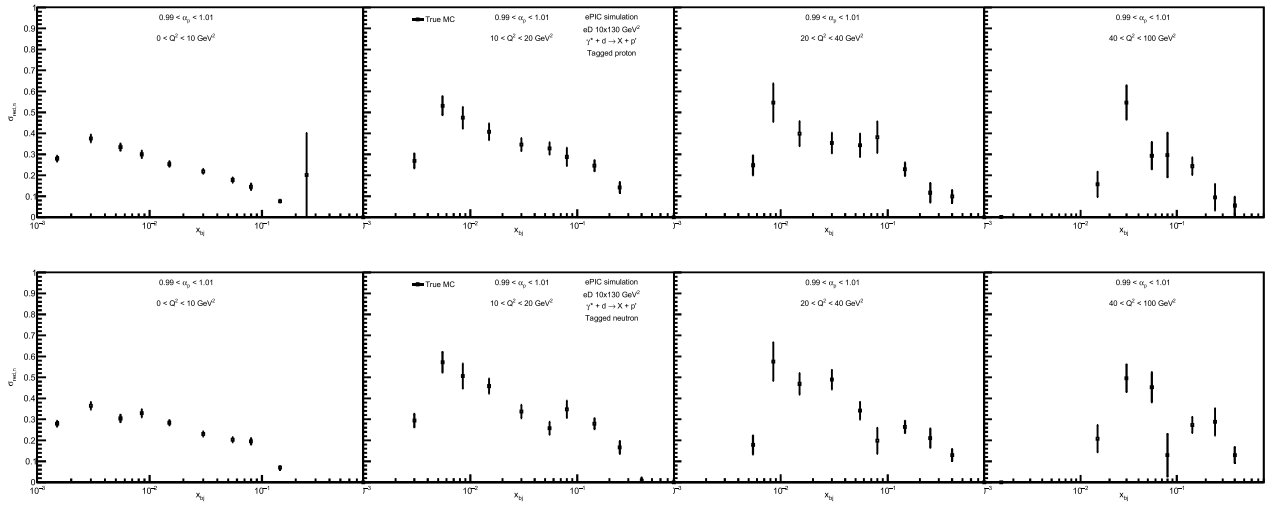

Figure C.7: Summary of the spectator reduced cross-sections extracted from the pole extrapolation procedure in bins of (x, Q^2). These are all evaluated for a $\mathcal{L}_{int} \sim 0.1 fb^{-1}$, which amounts to about 0.01 the total electron + deuteron luminosity expected during the early EIC running period.

C.5.3 He3 with double spectator tagging

Traditionally, neutron measurements have been done through light-nuclei target as there are no free neutron source. At ePIC, one can measure the scattering of a mostly free neutron inside D and He from using the far forward detectors to tag the spectator protons. Taking advantage of this technique, with the polarized ^{3}He beam planned in year 5 of early EIC running, the virtual photon spin asymmetry, A_1, and the spin dependent structure function, g_1, of neutrons can be measured with less model dependence and achieve more precise results. These are important for verifying nuclear effect, understanding the spin composition of nucleons, extracting the Bjorken sum and α_s via polarized measurement.

The asymmetry, A_1, is related to the longitudinal spin asymmetry as described in Sec. A.7, Eqns.7-10. R is the ratio of the longitudinal to transverse virtual photon absorption cross sections as defined in Eqn. 9, which can be extracted from the spin-independent structure functions. The spin-dependent structure function, g_1, is related to A_1 by this equation:

$$\frac{g_1(x,Q^2)}{F_1(X,Q^2)}(1+\gamma^2) = \gamma A_2(x,Q^2) + A_1(x,Q^2) \tag{20}$$

where the asymmetry A_2 can also be measured at EIC. Projection study of the sensitivity and kinematic coverage of A_1^n and g_1^n at early EIC running is done using the event samples generated by BeAGLE. It is assumed that half of the running time will be spent on the longitudinal spin asymmetry, $A_\parallel$, and the other half of the time on $A_\perp$. The statistical uncertainty of A_1 is then estimated from $\delta A_{\parallel,\perp} \approx \frac{1}{\sqrt{N} P_e P_N}$ where N is the number events in each x and Q^2 bin in the simulation. P_e and P_N are the polarization of the electrons and neutrons, which are both assumed to be 70% for this study.

The double spectator tagging is tested using a primitive method of checking the number of hits in the RP and OMD. The number of proton tracks are formed based on the minimum number of hits among

the planes of a detector. If there are at least two proton tracks, the event is tagged as *en* scattering. The simple tagging method has a uniform tagging efficiency of about 83% and purity above 90% across all x and Q^2 region, which can be further improved by vetoing neutron events in ZDC and the currently-under-development tracking algorithm for the spectator protons.

Figure C.8 shows the projected kinematic coverage and estimated statistical uncertainties of A_1^n and g_1^n measurement in year 5 of EIC running, where the A_1^n central values of the projected result are calculated from parameterizations of a world data analysis [41], and g_1^n values are approximated by $A_1 \cdot F_1$, where the structure function, F_1, is taken from the JAM22 global fit [55]. Highlighted region in yellow on the left is the rough region for the current existing data. ePIC will uncover a large phase space for new A_1^n and g_1^n data while reach low x region which is important for spin physics study and α_s extraction.

The A_1^n data are also extracted using the traditional method using a simple ^{3}He model:

$$A_1^{^3\mathrm{He}} = P_n \frac{F_2^n}{F_2^{^3\mathrm{He}}} A_1^n + 2P_p \frac{F_2^p}{F_2^{^3\mathrm{He}}} A_1^p \tag{21}$$

to compare the result from double tagging as shown in Fig. C.8. In the model calculation, the A_1s and F_2s are obtained from the same parameterizations and JAM22 global fit as earlier. The effective nucleon polarization, $P_n = 0.86 \pm 0.02$ and $P_p = -0.028 \pm 0.004$ in ^{3}He are obtained from [93]. By using the less model dependent double spectator tagging method, the uncertainties of the data are reduced by about 50 - 70%.

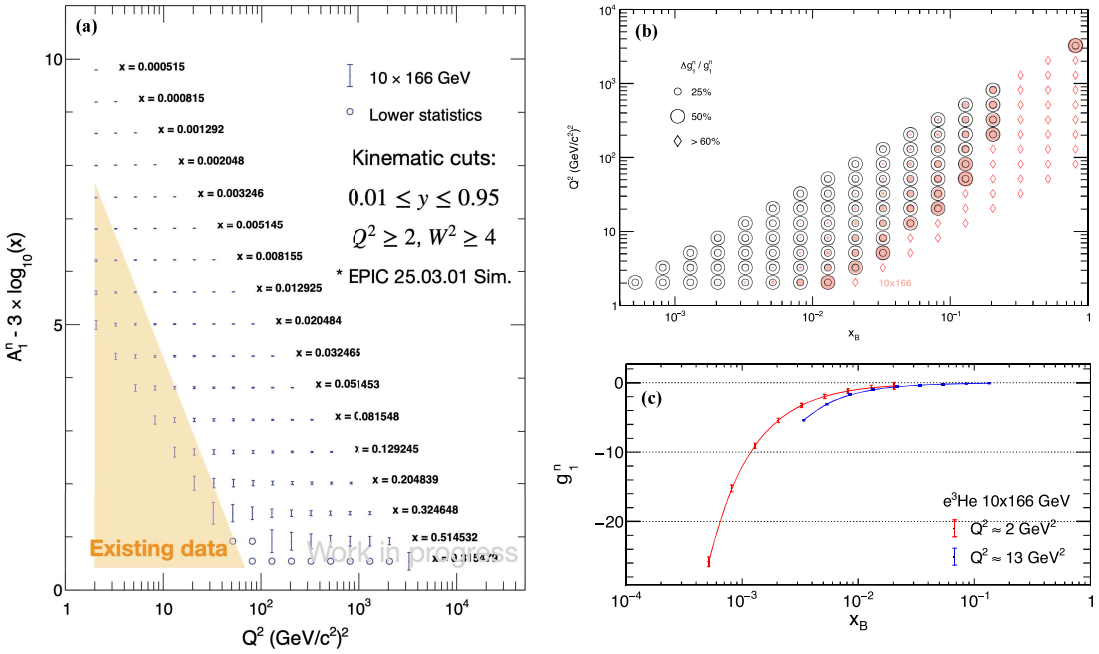

Figure C.8: (a) Projected result and statistical uncertainty on A_1^n in year five of EIC running using the double tagging method. Central bin A_1^n value is calculated from parameterization taken from [41]. Highlighted area is the roughly the region of the current existing data on A_1^n. (b) and (c): Projected result and statistical uncertainty on g_1^n.

C.5.4 Imaging program of heavy nuclei and saturation physics

The momentum transfer distribution ($|t|$) forms a diffractive pattern that encodes information about the spatial distribution of gluons in the hadron wave function [94]. Since $|t|$ is conjugate to the impact

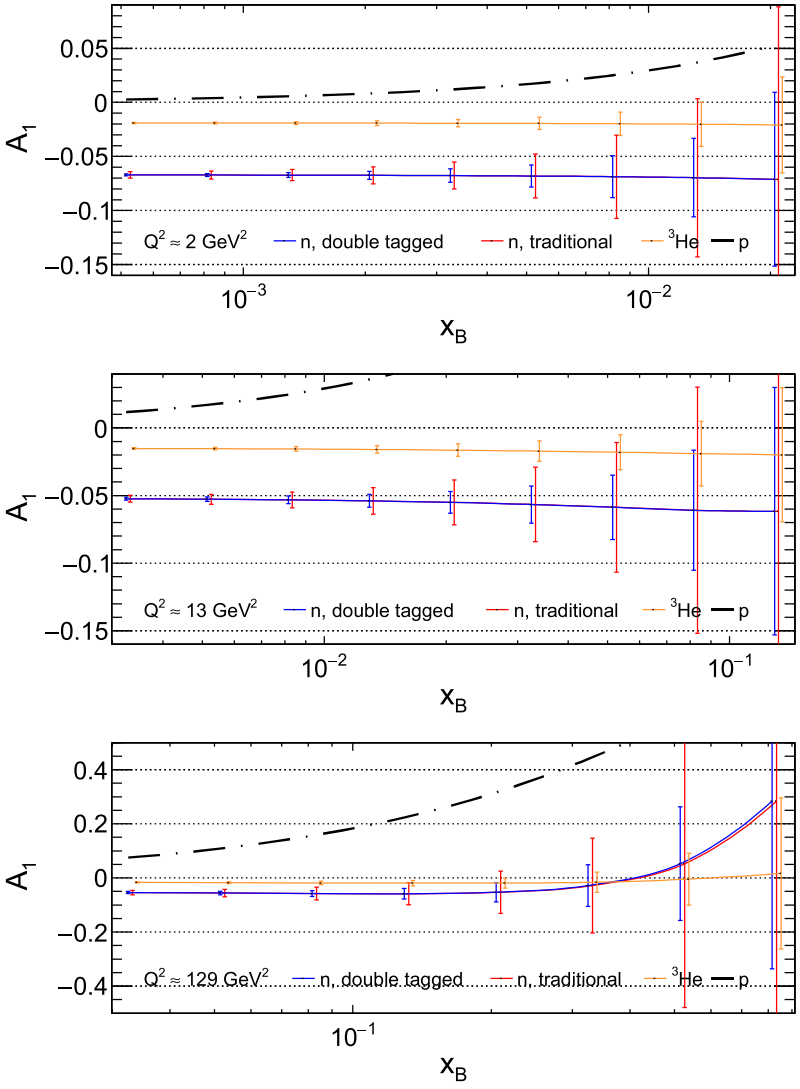

Figure C.9: Comparison of A_1^n uncertainties extracted using the traditional model dependent method (blue) versus the double tagging method (red) at three selected Q^2 bin. The orange line in each plot is the estimated statistical uncertainty of $A_1^{^3\mathrm{He}}$ while the black dashed line is the central value of A_1^p.

parameter, a Fourier-Bessel (Hankel) transformation of the distribution enables us to obtain the spatial profile of the gluon density. However, the $|t|$ distribution is a challenging measurement, as it depends on the outgoing nucleus' momentum, which, for heavy nuclei, we cannot access precisely. Consequently, we have to use different methods to reconstruct this measurement. There are two main complications with this: limited precision and a large background from incoherent production where the nucleus breaks up. This analysis utilizes a projective technique, as demonstrated in [67], to reconstruct the $|t|$ distribution by invoking cuts and momentum projection along the direction normal to the electron scattering plane ($\hat{n}$) to resolve the diffractive pattern and the resulting gluon distribution through a Fourier-Bessel transformation.

There are three different ways that we implement to reconstruct the $|t|$ distribution: method E which directly solves for $P_{\mathrm{A}'}$ to arrive at the final formula for $|t|$ and is used to generate MC events, method L uses a corrected outgoing ion momentum by using the mass as an additional constraint, and the projection

method which incorporates a wedge cut as an additional requirement for method L. Given a coherent exclusive diffractive VM event, we have the following conservation of four-momenta equation

$$P_e + P_{\mathrm{A}} \rightarrow P_{e'} + P_{\mathrm{A}'} + P_{\mathrm{VM}}, \tag{22}$$

where P_e is the four-momentum of the incoming electron, P_{A} denotes the four-momenta of the incoming ion, $P_{e'}$ and $P_{\mathrm{A}'}$ are the outgoing electron and ion four-momenta respectively, and P_{VM} is the four-momenta of the produced VM. The derivation of the different methods of $|t| = -(P_{A'} - P_A)^2$ reconstruction are based off of Eqn. 22 and more information about their derivation can be found in [95]. The derivation of the projection method is as follows:

- We define the projected $|t|$ as

$$|t|_{\mathrm{proj}} = (t_x, t_{\hat{n}}, t_z, t_E), \tag{23}$$

  where

$$\begin{aligned} |t|_{\hat{n}} &= -[(P_e - P_{e'} - P_{\mathrm{VM}}) \cdot \hat{n}]^2 \\ &= (P_{\mathrm{VM}} \cdot \hat{n})^2. \end{aligned} \tag{24}$$

  - Beginning with the $|t|$ distribution given by method L, we decompose as $|t| = |t|_{\perp} + |t|_{//}$ where $|t|_{\perp} = |t|_x + |t|_y$ and $|t|_{//} = |t|_z + |t|_E$ are transverse and longitudinal components respectively.
  - We further decompose the transverse components such that $p_x = \sqrt{|t|_x}$ and $p_y = \sqrt{|t|_y}$ (i.e. $p_y = p_{\hat{n}} = \sqrt{|t|_y} = \sqrt{|t|_{\hat{n}}}$ given the relation $|t|_{\perp} = p_{\perp}^2 = p_x^2 + p_y^2$).
  - We then parameterize p_x and p_y for which

$$\begin{aligned} p_x &= p_{\perp} \sin(\theta) \\ p_y &= p_{\perp} \cos(\theta). \end{aligned} \tag{25}$$

  - Lastly, we cut a wedge of angle θ_{max} from the $p_y = p_{\hat{n}}$ axis (see [67] for more details). The angle for the wedge cut is given by

$$\theta_{\mathrm{max}} = \tan^{-1}\left(\sqrt{\frac{|t_x|}{|t_{\hat{n}}|}}\right). \tag{26}$$

After constructing the momentum transfer profile, we can take a Fourier-Bessel transformation to extract the spatial distribution of the gluons [68]. As shown in [96], a 2-dimensional transformation of the transverse $|t|$ distribution gives the transverse distribution of the spatial profile. The transformation used is given by

$$F(b) \propto \frac{1}{2\pi} \int_0^{\infty} dq_{\mathrm{T}} q_{\mathrm{T}} J_0(b q_{\mathrm{T}}) \sqrt{\frac{d\sigma}{d|t|}}, \tag{27}$$

where J_0 is a Bessel function of the first kind, q_T is the transverse momentum, b is the impact parameter, and $d\sigma/d|t|$ is the differential cross section.

The results of this reconstruction are shown in Fig. C.10. First, we can see a significant enhancement in resolving the diffractive pattern of the $|t|$ distribution. Previously, the best method available for us to use was method L as stated in [95]. The projection method enables us to determine the peaks and minima with a much better resolution than before. The price we pay for making the wedge cut in the projection method is a loss of statistics, as shown in Fig. C.10. In this example, we use $\theta_{max} = \pi/12$ which results in $\approx$ 83% of lost coherent VM events. Second, the transformation shown in Fig. C.10 clearly indicates an improvement from the method L reconstruction. This analysis demonstrates that the projection method used to reconstruct the momentum distribution is an effective approach to overcome the previous challenges of the $|t|$ measurement and allows more precise spatial imaging of the gluons inside the nucleus.

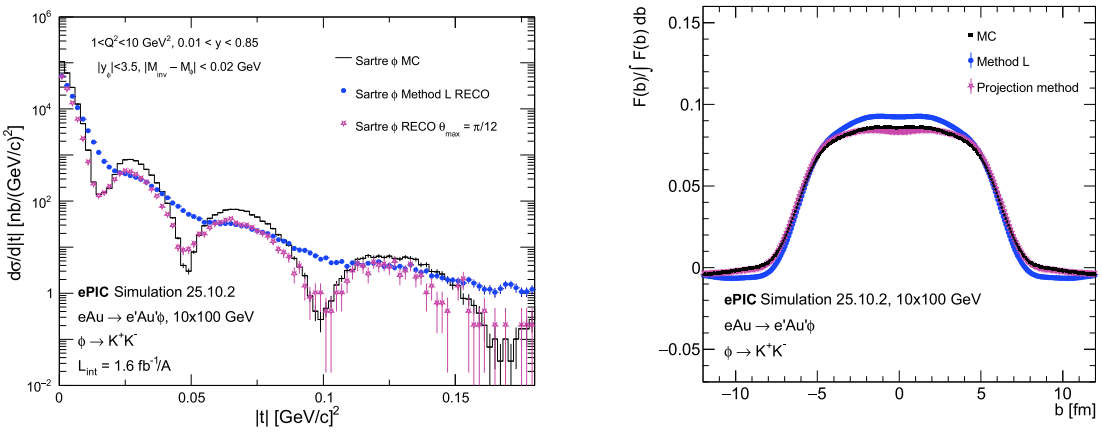

Figure C.10: Left: $|t|$ distribution with the method L and the projection method shown for comparision with the MC truth distribution (black curve). The filled blue circles represent method L reconstruction and the open pink stars correspond to reconstruction using the projection method with a wedge cut of $\theta_{\max} = \pi/12$. Note that the $|t|$ distribution that implements the projection method is normalized by $(\pi/2)/\theta_{\max}$ Right: 2-dimensional Fourier-Bessel transformation of the $|t|$ distribution with wedge cut of $\theta = \pi/12$. This shows the gluon spatial distribution with a comparison from the transforms of the truth, method L, and the projection method distributions. The black solid squares represent the truth distribution, the blue full circles correspond to $|t|$ reconstruction using method L, and the open pink stars represent the reconstruction of $|t|$ using the new projection technique.

C.6 Kaon Structure Function Studies and Far-Forward Λ^0 Reconstruction

C.6.1 Kaon Structure Function Motivations

The kaon is the lightest and simplest hadronic system containing a strange quark, making it a valuable probe for studying the influence of quark mass on hadron structure. Although theoretical calculations predict clear differences between the partonic structure of the pion and the kaon [97], particularly in the momentum carried by quarks and gluons, experimental information on the kaon structure remains very limited. The only measurement available is a Drell–Yan determination of the kaon-to-pion structure function ratio [98]. An alternative approach to access the kaon structure is provided by semi-inclusive measurements of the Sullivan process in deep-inelastic electron–proton scattering [99]. In this process, the electron scatters off the virtual kaon cloud of the proton, leading to final states containing strangeness such as $e + p \to e' + k^+ + \Lambda^0$. The future Electron–Ion Collider (EIC) setup, together with the ePIC detector, could provide the luminosity, kinematic coverage, and forward detection capabilities required to perform such innovative measurements. This study focuses on the projection of the expected uncertainties.

C.6.2 Kaon Structure Function Simulations

The feasibility of kaon structure measurements using the Sullivan process, as well as projections of the expected statistical uncertainties, were evaluated through detailed simulations. An event generator was developed to produce realistic events for the reaction of interest, $e + p \to e' + k^+ + \Lambda^0$, using state-of-the-art evaluated data. Simulations were performed for representative EIC beam-energy configurations, including 5×41, 10×100, 10×130, and 18×275 GeV. The transport of the final-state particles through

the ePIC detector was simulated using GEANT4, taking into account the detector geometry and response.

C.6.3 Kaon Structure Function Analysis

In the framework of a semi-inclusive measurement, the simulation analysis focused on the reconstruction of the Λ^0 hyperon. Since the calorimetric response to this neutral particle is indistinguishable from that of neutrons, its identification relies on signatures from its decay products. Indeed, the typical boost values of Λ^0 at EIC let it fly several meters along the forward region of ePIC, before it decays either via the charged channel $\Lambda^0 \to p + \pi^-$ (64%) or via the neutral channel $\Lambda^0 \to n + \pi^0 \to n + \gamma_1 + \gamma_2$ (36%) [23]. As the charged decay channel is sensitive to the magnetic fields present in the experimental setup, the first stage of the analysis focused on the reconstruction of Λ^0 through the triple coincidence $n + \gamma_1 + \gamma_2$.

The simulation analysis was performed using the reconstruction framework EICRECON. This software package already includes a Λ^0 reconstruction module based on the detection of neutral decay products in the Zero-Degree Calorimeter (ZDC). While this method has been shown to be efficient for mono-energetic and mono-angular Λ^0 gun simulations [100], it proves largely inefficient when applied to realistic Λ^0 distributions generated by the event generator. Owing to the broad energy and angular distributions of the produced Λ^0 hyperons and decay products, combined with the limited geometric acceptance of the ZDC (positioned 35 m downstream of the interaction point), only a negligible fraction of events can be successfully reconstructed. This effect is illustrated in Fig. C.11.

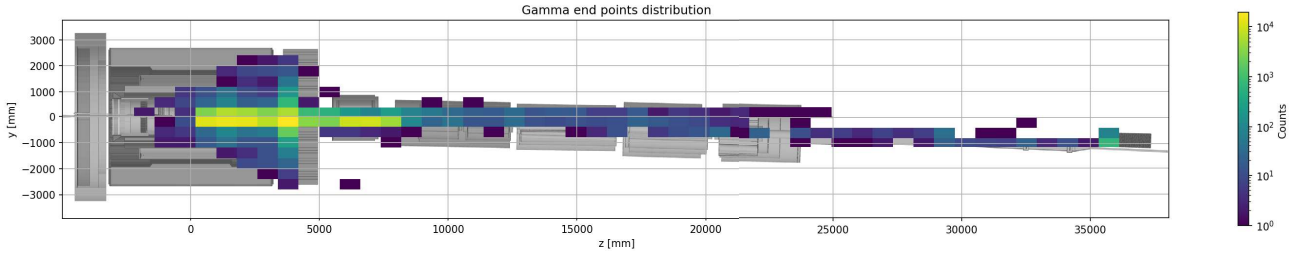

Figure C.11: Distribution of γ-ray impact points from the neutral decay of Λ hyperons in the forward region of ePIC at $5x41$ GeV. The acceptance of the ZDC alone, located 35 m downstream of the interaction point, is insufficient to ensure efficient Λ reconstruction. By additionally considering EndcapP, B0Ecal, and LFHCAL, a significantly larger fraction of neutral decay products can be intercepted, thereby substantially improving the reconstruction capability.

The EICRECON reconstruction module was therefore extended to search for neutral decay products not only in the ZDC, but also in three additional calorimeters located in the forward region of the ePIC setup: EndcapP, LFHCAL, and B0. EndcapP and LFHCAL predominantly intercept neutral decay products originating from low-energy Λ^0, which tend to decay closer to the interaction point. In contrast, B0 and the ZDC are primarily responsible for the detection of decay products from high-energy Λ^0 emitted into the far-forward region.

The energy spectrum of reconstructed Λ hyperons produced via the Sullivan process, in the 10×100 GeV beam energy configuration, is shown in Fig. C.12. Despite a relatively small reconstruction efficiency of approximately 1‰, the reconstructed spectrum closely follows the event generator prediction (shown as a black dashed line after afterburner treatment) and exhibits very high purity, with only a small residual background contribution.

These encouraging results are expected to improve further with the inclusion of the charged decay channel. Final projections of the anticipated statistical uncertainties on the kaon structure function at EIC/ePIC will be presented in a forthcoming dedicated study.

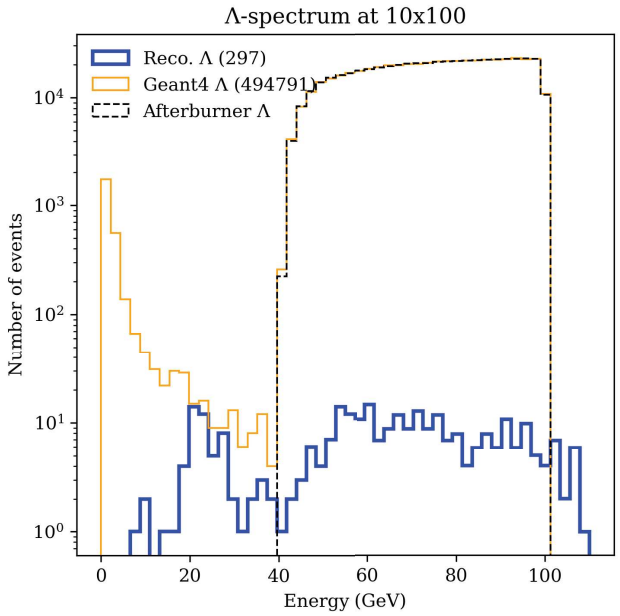

Figure C.12: Energy spectrum of Λ hyperons in the 10 × 100 GeV configuration. The black dashed line represents Λ hyperons from the event generator after the afterburner treatment. The yellow line corresponds to Geant4 truth-level Λ hyperons, including secondary contributions. The blue line shows the reconstructed Λ candidates in ePIC using the upgraded EICRECON algorithm, leveraging EndcapP, LFHCAL, B0Ecal, and ZDCHcal information. While no Λ hyperons could be reconstructed using ZDC information alone, the upgraded algorithm achieves a high-purity reconstruction.

C.7 Summary

This appendix presents the early science prospects for the exclusive physics program during Phase I of the Electron-Ion Collider (EIC). The focus is on leveraging high-luminosity electron-proton and electron-nucleus collisions to explore the fundamental structure of hadrons and nuclei through exclusive processes. These reactions, where all final-state particles are measured, offer clean access to the underlying dynamics of strong interactions.

The Phase I running plan provides a diverse range of beam species, energies, and polarization configurations, enabling precision studies of exclusive reactions across a wide kinematic range. Light nuclei, such as deuterium and helium-3, allow for unique probes of nucleon and nuclear structure, while heavy ions like gold facilitate studies of coherence and diffractive phenomena.

It also outlines the expected experimental conditions and integrated luminosities, along with simulation-based projections that demonstrate the feasibility and impact of the early exclusive measurements. These results will lay the groundwork for the EIC's long-term physics goals and help establish the collider as a leading facility for exploring the quantum structure of matter.